Structural Engineering and Mechanics, Vol. 37, No. 3 (2011) 267-283 267
DOI: http://dx.doi.org/10.12989/sem.2011.37.3.267

Quasi-static cyclic displacement pattern for seismic evaluation of reinforced concrete columns

E. Yüksel*[1] and M. Sürmeli[2]

[1]*Faculty of Civil Engineering, Istanbul Technical University, Maslak-Istanbul, Turkey*
[2]*Graduate School of Istanbul Technical University, Maslak-Istanbul, Turkey*

(Received October 2, 2008, Accepted October 13, 2010)

Abstract. Although earthquakes generate random cyclic lateral loading on structures, a quasi-static cyclic loading pattern with gradually increasing amplitude has been commonly used in the laboratory tests because of its relatively low cost and simplicity compared with pseudo-dynamic and shake table tests. The number, amplitudes and sequence of cycles must be chosen appropriately as important parameters of a quasi-static cyclic loading pattern in order to account for cumulative damage matter. This paper aims to reach a new cyclic displacement pattern to be used in quasi-static tests of well-confined, flexure-dominated reinforced concrete (RC) columns. The main parameters of the study are sectional dimensions, percentage of longitudinal reinforcement, axial force intensity and earthquake types, namely, far-fault and near-fault.

Keywords: reinforced concrete column; seismic evaluation; loading pattern; displacement pattern; quasi-static loading.

1. Introduction

Numerous experimental studies have been conducted on structures or structural components in order to understand their response to earthquakes. In these studies, quasi-static cyclic loading has generally been used due to its simplicity and relatively low cost compared with pseudo-dynamic or shake table tests.

Krawinkler (1996) revealed that in order to utilize results obtained from quasi-static cyclic load tests on structural components for a general performance evaluation, it is necessary to establish loading histories that capture critical issues of component capacity, as well as seismic demands. Due to cumulative damage matter, the capacity depends on the number of inelastic excursions and the magnitude of each excursion. These two parameters strongly depend on the frequency content of the ground motion, the periods of the structure, and the strength and inelastic deformation characteristics of the structure. Kawashima *et al*. (2002) stated that the loading history applied to a column specimen generally consists of stepwise increasing deformation cycles with constant increment of δ_y. They also declared that there is disagreement among researchers concerning the number of cycles in each loading displacement, and those factors determining the number of cycles and the constant displacement increment of δ_y in the loading history are unknown. Although the

*Corresponding author, Assistant Professor, E-mail: yukselerc@itu.edu.tr

number of cycles has often been assumed to be three in recent experimental studies involving ductile RC columns, there are very few studies investigating how to determine the loading history for cyclic loading tests. Previous studies tried to determine a standard loading history for quasi-static cyclic loading tests of RC bridge columns. Nonlinear time history analyses (NTHA) were performed for various SDOF systems with many earthquake records. Analytical results obtained from these studies were evaluated in terms of the number of inelastic excursions and the sum of the normalized plastic deformation ranges. The loading histories for cyclic loading tests were proposed on the basis of statistical studies of the inelastic excursions.

Shafei and Zareian (2008) developed quasi-static loading protocols for displacement-sensitive nonstructural components. The developed quasi-static loading protocols help to predict the probable behavior of displacement-sensitive nonstructural components during an earthquake more accurately by considering the loading history characteristics of the seismic event. Tsuno and Park (2004) developed a procedure to estimate the damage and failure of a column caused by a seismic loading. Five specimens were tested using uni-directional and bi-directional cyclic load patterns combined with a constant axial load. They showed that the displacement amplitude in cyclic loading starts at a small level and increases the energy dissipation capacity of a column in a step-by-step manner until the ultimate state is the same for both uni-directional and bi-directional loading. However, if an extremely large displacement is applied to a column at the early stage of a cyclic loading, it may lead to buckling of the longitudinal bars and confinement failure with only small energy dissipation. Gatto and Uang (2003) conducted wood frame shear wall tests using different loading protocols. They stated that the load sequence has a significant influence on shear wall performance. Krawinkler *et al*. (2000) developed two loading histories namely basic and near-fault loading history for testing of steel beam-to-column assemblies. Time history analyses were performed for 3, 9 and 20 stories SAC model buildings for calculating demand parameters. In order to convert the response time history of the interstory drift angle, as a deformation parameter to be used to control the loading history, cycle counting was used. Kawashima and Koyama (1988) reported the effect of discrete cyclic load patterns on the response of RC bridge columns. They showed that the greater the number of loading cycles for the same displacement, the smaller the maximum displacement of the column before its ultimate state was achieved. However, the ultimate strength of the tested column was not affected to any considerable extent by the loading pattern used in the study. They also stated that there is limited knowledge concerning the effect of different loading patterns, and that the damage accumulation of an RC column with different loading patterns is not clearly understood. Hwang and Scribner (1984) studied the effect of loading history on RC cantilever beams. They showed that the sequence of application of large and small deformations had a relatively negligible effect on the cyclic behavior of the members. The most significant factor was the maximum displacement the members experienced.

ATC-24 (1992) outlines guidelines for cyclic seismic testing of components of steel structures. A cumulative damage concept on which the selection of loading histories is based has been developed and a loading history was recommended that consists of stepwise increasing deformation cycles. As part of the initial work on the next generation performance based design project, interim recommended protocols for testing of structural and nonstructural components and systems found in buildings were documented in FEMA 461 (2007), for the purpose of establishing fragility functions of the components.

The purpose of this study was to develop a new quasi-static cyclic displacement pattern for well-confined flexure-dominated RC columns. The experimentally approved hysteretic and damage models were utilized in the study. The main parameters are the sectional dimensions, percentage of longitudinal reinforcement, axial force intensity and earthquake type namely far-fault and near-fault effects. For several columns having the listed parameters, the cumulative damage obtained from the proposed quasi-static cyclic displacement pattern and the commonly used quasi-static cyclic displacement patterns in which one or three cycles are repeating at each ductility level, are compared with those obtained from NTHA performed for the several earthquake acceleration records.

2. Definition of RC columns and sectional parameters

Several full-scale cantilever type columns that had different sectional dimensions and percentages of longitudinal reinforcement were tested in the laboratory (Karadogan *et al*. 2006). The height of the columns was 4.0 m. Typical column elevation and cross section are shown in Fig. 1. The cross section consists of 8 main bars with one hoop and 2 ties. Transverse reinforcements are located at Φ8/10 in the confinement zone, which is the lower 1.60 m of the column height, and at Φ8/15 in the remaining part. The design strength was 45 MPa and 420 MPa for concrete and re-bars, respectively. The axial load was constant at about 5% of the column capacity for all specimens. The columns were tested in the quasi-static manner using the cyclic displacement pattern which is used in the laboratory as standard loading pattern. The loading pattern consists of three times repeated gradually increasing displacement cycles. In this paper, the existing column test results were only used for the calibration of the hysteretic models and the evaluation of the utilized cumulative damage model.

Given an earthquake acceleration record, the response history of a column was determined using the inelastic dynamic analysis program IDARC (Reinhorn *et al*. 2006). IDARC computes the response of the column by taking into account the degradation in stiffness, lateral strength and energy dissipation capacity, which occur as inelastic deformations progress over the course of the earthquake action. The degree of stiffness and strength degradation and pinching are controlled by some parameters in the Smooth Hysteretic Model (SHM) used in IDARC. The SHM parameters

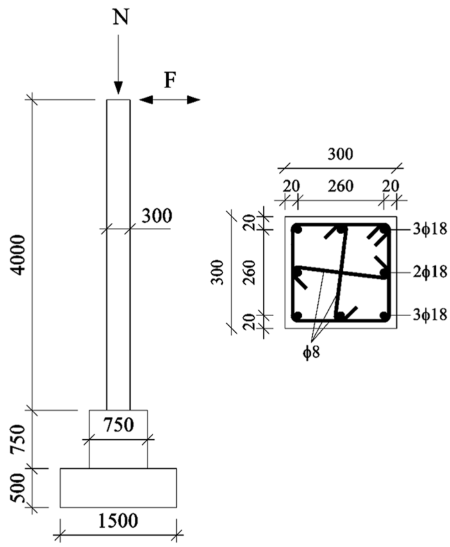

Fig. 1 Elevation and cross section of the tested columns (all dimensions in mm)

used in this study are $\alpha = 4$, $\beta_1 = 0.10$, $\beta_2 = 0.12$, $R_s = 0.13$, $\sigma = 0.06$, $\lambda = 0.60$, $N = 2$, and $\eta = 0.49$, which were attained from the calibration process with the experimental results (Surmeli 2008).

To demonstrate the success of the modeling process, base shear versus top displacement hysteresis obtained in experimental and analytical studies for a representative column that had a cross section of 40 × 40 cm is shown in Fig. 2.

The column sectional dimensions used in the analytical work were 30 × 30, 40 × 40, 50 × 50 and 60 × 60 cm. For each sectional dimension, three longitudinal reinforcement ratios, ρ_v, of 1%, 2% and 3% were selected. The three different axial force intensities of 5, 10 and 15% of the axial load capacity of the columns were used. A general outline of the selected parameters is given in Table 1, (Yuksel and Surmeli 2010). The mass used in NTHA was concentrated at the top of the column and it was calculated from the corresponding axial force intensity of the column.

The material characteristics used in the analytical work are as follows: For unconfined concrete, compressive strength is 40 MPa, strains at the peak stress and the crushing are 0.002 and 0.004, respectively. For confined concrete, compressive strength is 46.0 MPa and strain at crushing is 0.015. For steel, the yield stress is 420 MPa, the maximum stress 550 MPa, the hardening and ultimate strains are 0.008 and 0.10, respectively.

The software XTRACT (2006) is employed for the cross-sectional analyses and producing the

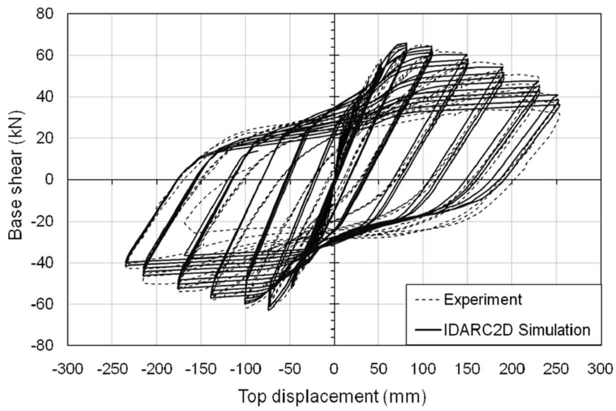

Fig. 2 Comparison of experimental and analytical results for a representative column

Table 1 Sectional parameters

ρ_v	N/N_0	Cross sectional dimensions (cm×cm)			
1%	5% 10% 15%	30×30	40×40	50×50	60×60
2%	5% 10% 15%	30×30	40×40	50×50	60×60
3%	5% 10% 15%	30×30	40×40	50×50	60×60

Table 2 Capacities and vibration periods of theoretical columns

Column	M_y (kNm)	M_u (kNm)	Δ_y (mm)	Δ_u (mm)	T (sec)	μ_0	Ductility Range
C-60-%3-2160	1537	1561	45	150	0.95	3.3	$3.3 < \mu_0 < 4.8$
C-50-%3-1500	870	886	53	195	1.16	3.7	
C-60-%2-2160	1214	1237	44	163	1.06	3.7	
C-60-%3-1440	1446	1499	45	173	0.81	3.8	
C-50-%2-1500	689	704	51	210	1.28	4.1	
C-50-%3-1000	824	854	54	225	0.99	4.2	
C-40-%3-960	435	447	63	267	1.45	4.2	
C-60-%1-2160	867	888	42	182	1.22	4.3	
C-60-%2-1440	1113	1159	43	193	0.90	4.5	
C-60-%3-720	1305	1427	43	198	0.59	4.6	
C-50-%1-1500	491	504	50	233	1.47	4.7	
C-40-%3-640	418	434	66	312	1.24	4.7	
C-40-%2-960	343	352	62	296	1.62	4.8	$4.9 < \mu_0 < 6.1$
C-50-%2-1000	637	663	51	254	1.10	5.0	
C-30-%3-540	169	174	83	416	2.02	5.0	
C-50-%3-500	742	815	49	257	0.70	5.2	
C-60-%1-1440	760	786	41	226	1.06	5.5	
C-40-%1-960	242	249	59	329	1.88	5.6	
C-30-%3-360	165	170	89	501	1.73	5.6	
C-30-%2-540	134	138	79	447	2.22	5.7	
C-40-%2-640	320	333	63	359	1.39	5.7	
C-40-%3-320	379	417	63	369	0.90	5.9	
C-60-%2-720	958	1068	38	228	0.64	6.0	
C-50-%1-1000	432	449	49	301	1.28	6.1	
C-50-%2-500	552	614	49	311	0.81	6.3	$6.2 < \mu_0 < 10.4$
C-30-%3-180	151	162	87	562	1.27	6.5	
C-30-%2-360	126	131	84	547	1.92	6.5	
C-30-%1-540	95	99	75	516	2.54	6.9	
C-40-%1-640	213	222	58	412	1.63	7.1	
C-40-%2-320	281	308	61	445	1.03	7.3	
C-60-%1-720	607	667	39	303	0.81	7.8	
C-30-%2-180	113	123	82	696	1.42	8.5	
C-30-%1-360	85	90	75	682	2.21	9.1	
C-50-%1-500	350	380	46	419	0.99	9.1	
C-40-%1-320	176	188	58	565	1.26	9.7	
C-30-%1-180	71	76	76	790	1.71	10.4	

moment curvature envelopes for the column sections. Default models of XTRACT which are Mander unconfined and confined concrete models, and bi-linear with a parabolic strain hardening steel model were used in the calculation of moment-curvature envelopes.

Table 2 shows the calculated M_y yield and M_u ultimate moment capacities. The Δ_y yield and Δ_u maximum lateral top displacements were determined by performing pushover analyses. The

Table 3 Earthquake records

Far-Fault Earthquake Records	Near-Fault Earthquake Records
1, 2- Kocaeli 17/08/1999 Düzce S. DZC180, DZC270	1, 2- nf01, nf02 (Tabas) 16/09/1978 Tabas S.
3- Adana-Ceyhan 27/06/1998 Ceyhan S. East	3, 4- nf03, nf04 (Loma Prieta) 18/10/1989 Los Gatos S.
4- Bingöl 01/05/2003 Bingöl S. North	5, 6- nf05, nf06 (loma Prieta) 18/10/1989 Lex Dam S.
5- W. Washington 13/04/1949 Olympia S. Com (86)	7, 8- nf07, nf08 (C. Mendocino) 25/04/1992 Petrolia S.
6- S. Fernando 09/02/1971 24278 Castaic S. ORR291	9, 10- nf09, nf10 (Erzincan) 13/03/1992
7- Imp. Valley 15/10/1979 5053 Calexico S. CXO225	11- nf12 (Landers) 28/06/1992 24 Lucerne S.
8- Imp. Valley 15/10/1979 5055 Holtville S. H-HVP225	12, 13- nf13, nf14 (Northridge) 17/ 01/1994 77 Rinaldi Re St.
9- Coyote Lake 06/08/1979 Gilroy Array #4 San Yas. School	14, 15- nf15, nf16 (Northridge) 17/ 01/1994 24514 Sylmar
10, 11- Coalinga 02/05/1983 36456 Parkfield S.	16, 17- nf17,nf18 (Kobe) 16/01/1995
12, 13- Chalfant Valley 07.21.1986 54428 Zack Brothers Ran.	18, 19- nf19, nf20 (Kobe) 16/01/1995 Takatori S.
14,15- Friuly 06/05/1976 8012 Tolmezzo S. TMZ000, TMZ270	20- Kocaeli 17/08/1999 Yarımca S. YPT060
16,17- Victoria 6604 09/06/1980 Cerro Prieto S.	21- Kocaeli 17/08/1999 Sakarya S. East
18, 19- Whittier Narrows 01/10/1987 24436 Tarzana, Cedar Hill	22, 23- Düzce 12/11/1999 Düzce S. DZC180, DZC270
20- Alkion-Greece 24/02/1981 Korinthos-OTE Build. Dir. Y	24- Chi-Chi Taiwan 20/09/1999 CHY080-West
21- Campano Lucano 23/11/1980 Sturno S. Dir.(Y)	25- Northridge 17/01/1994 0637 Sepulveda VA S. SPV360
22- South Iceland 17/06/2000 Thjorsarbru S. Dir.(Y)	26, 27- Northridge 17/01/1994 74 Sylmar - Converter Sta
23- Avej 22/06/2002 Avej(Bakhshdari) S. Dir.(X)	28, 29- Northridge 17/01/1994 24279 Newhall - Fire Sta
24- Taiwan Smart 20/05/1986 29 SMART1 M07 St. 40M07NS	30- Northridge 17/01/1994 24207 Pacoima Dam (upper left)
25- Superstition Hills(B) 24/11/1987 5061 Calipatria Fire Station	31- Northridge 17/01/1994 Sylmar - County Hosp.Park. Lot
26- Spitak 07/12/1988 12 Gukasian S. GUK000	32, 33- Superstition Hills 24/11/1987 5051 Parach. Test Site
27- 28- Irpinia 23/11/1980 Sturno S. STU270, STU000	34, 35- Imp. Valley 15/10/1979 942 El Centro Array #6
29- 30- North Palm Springs 12204 08/07/1986 San Jacinto	36, 37- Imp. Valley 15/10/1979 Meloland H-EMO000
31- 32- Kiholo Bay, Hawai`i Island 15/10/2006 Hawaii Honokaa	38- Morgan Hill 24/04/1984 57217 Coyote Lake Dam
33- 34- El Salvador 13/01/2001 Observatorio S. Com (180), (90)	39, 40- Gazli,USSR 17/05/1976 9201 Karakyr GAZ090-000
35- 36- Landers 28/06/1992 23 Coolwater S. CLW-LN &TR	
37- 38-Northridge 17/01/1994 24538 Santa Monica City Hall	
39- 40- Northridge 17/01/1994 224400 LA - Obregon Park	

corresponding displacement ductility of each column is calculated as $\mu = \Delta_u/\Delta_y$. The obtained displacement ductilities are classified into three groups, each possessing an equal number of columns. The vibration periods T given in the table is calculated by using the pre-yield flexural stiffness of the bi-linearized moment-curvature relations. The abbreviation C-60-%3-2160 represents a column having the cross section of 60 × 60 cm, a longitudinal reinforcement ratio of 3% and subjected to 2160 kN compression force, which is almost 15% of the column axial force capacity.

3. Earthquake records

Eighty earthquake acceleration records from various stations (SAC 1997, PEER 2000, TKYHP, COSMOS, Ambraseys *et al.* 2002 and USGS) around the world listed in Table 3 were used as input ground motions in NTHAs. Different characteristics were considered when selecting the records, such as PGA, PGV and closeness to the fault line. Half of the records involve a far-fault type and the other half a near-fault type. All of the near-fault ground motions are obtained from stations that are located less than 8.9 km from the fault line, and the corresponding PGV values ranged from 43.9 to 173.8 cm/sec. PGA of near-fault records varied between 263 to 1260 cm/sec^2. The PGA of far-fault earthquakes ranged from 195.2 to 866.2 cm/sec^2 and PGV values varied from 9.2 to 58.8 cm/sec. The surface wave magnitude (M_s) changes between 5.7 and 7.8 for the overall strong motion data set.

The elastic response spectrum curves for all the records were calculated using Seismosignal (2006). Five percent of the critical damping was used in the analyses. The calculated spectral curves for far-fault and near-fault earthquake types are shown by gray lines in Figs. 3 and 4. The average spectra and spectra defined by the Turkish Seismic Code (2007) for rock and soft soils are also given in the same figures.

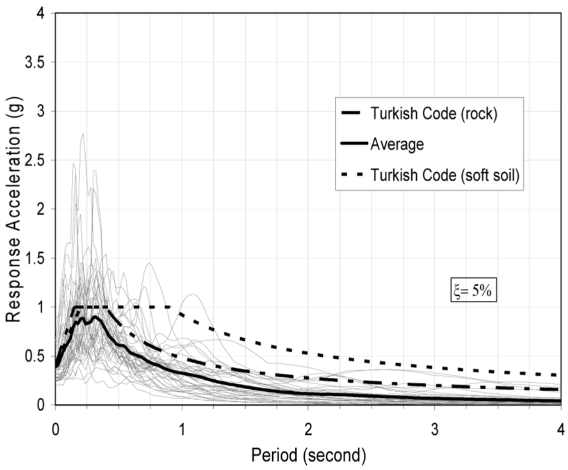

Fig. 3 Elastic response spectra for far-fault ground motions

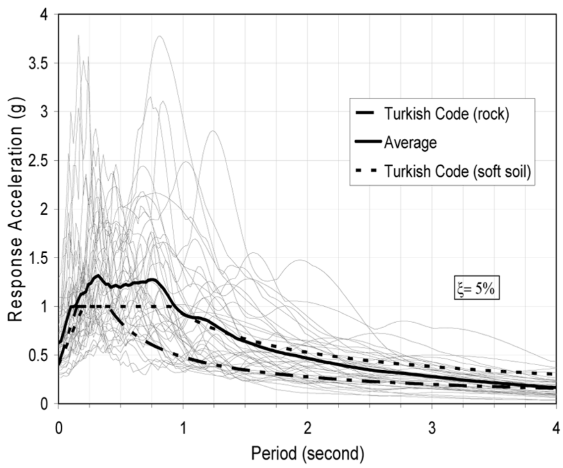

Fig. 4 Elastic response spectra for near-fault ground motions

4. Damage models

Krawingler (1996) showed that damage in a component is cumulative and that the level of damage depends not only on the maximum deformation, but also on the history of deformations the component undergoes before and after the occurrence of the maximum deformation. Thus, cumulative damage concepts have to be utilized to assess performance.

Among the many damage models available in the literature for cumulative damage assessment of RC components subjected to seismic excitations, the Park and Ang damage model seems to be the most promising due to its simplicity and extensive calibration against experimentally observed seismic damage in RC structures. The Park and Ang damage index is a linear combination of the maximum ductility and the hysteretic energy dissipation demand imposed by an earthquake on a structure (Park and Ang 1985). The damage (DI) represented by this model is expressed in Eq. (1).

$$DI = \frac{\delta_m}{\delta_u} + \frac{\beta}{\delta_u P_y}\int dE_h \tag{1}$$

where δ_m is the maximum experienced deformation, δ_u is the ultimate deformation capacity under static loading, P_y is the yield strength of the component, and the $\int dE_h$ integral represents the hysteretic energy absorbed by the element during the response history. The dimensionless parameter of β represents dissipated hysteretic energy contribution to the damage of a component. A value of β 0.1 was suggested for the nominal strength deterioration (Park *et al.* 1987). The model has been calibrated with the observed structural damage of several RC buildings (Park *et al.* 1985). DI < 0.4 represents reparable damage, 0.4 < DI < 1.0 represents damage that is beyond repair, and DI > 1.0 represents total collapse.

To confirm the success of the Park and Ang damage model, it was applied to a representative tested column that had a cross section of 40 × 40 cm and it estimated a damage index of 0.895. The calculated damage index is highly consistent with the observed damage state of the column in the experimental study (Table 4).

The sum of normalized plastic deformation ranges constitutes another index to represent the cumulative damage. The sum of normalized plastic deformation ranges is defined as

$$NP = \sum(\delta_i - \delta_y)/\delta_y \tag{2}$$

Table 4 Comparison of experimental damage with the damage index of Park & Ang

Section	Photograph	Observed Damages	Calculated DI
40×40		Buckling of longitudinal reinforcement, crushing of confined concrete, average plastic zone length is 35 cm.	0.895

in which *NP* is the sum of normalized plastic deformation ranges; δ_i is i^{th} absolute peak displacement response larger than the yield displacement before the maximum absolute displacement observed and δ_y is yield displacement.

For columns used in the analytical work, dominant vibration period which is calculated by using

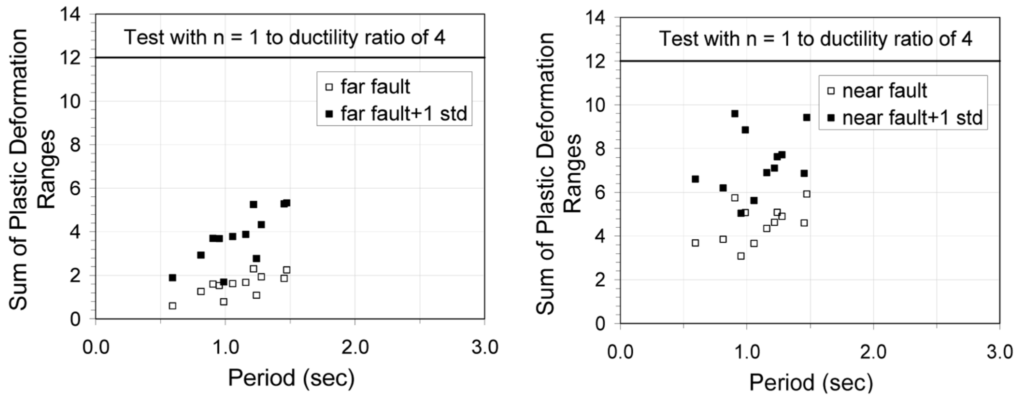

Fig. 5 Vibration period versus NP relationship for $3.3 < \mu < 4.8$

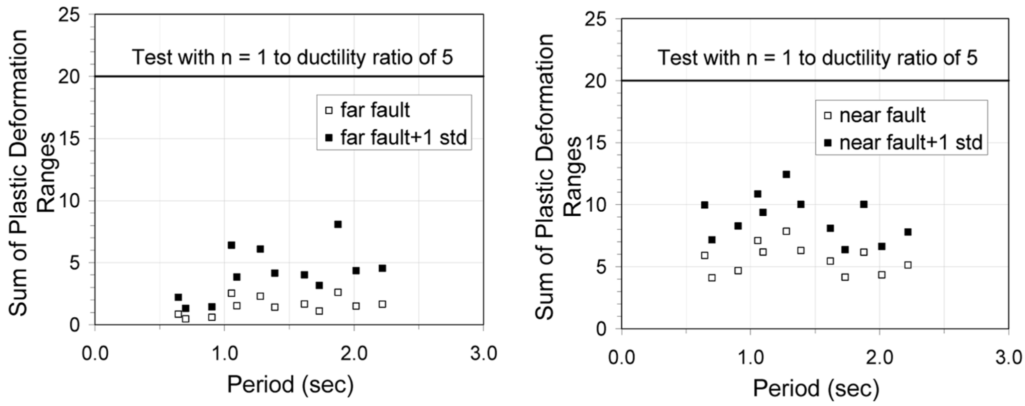

Fig. 6 Vibration period versus NP relationship for $4.9 < \mu < 6.2$

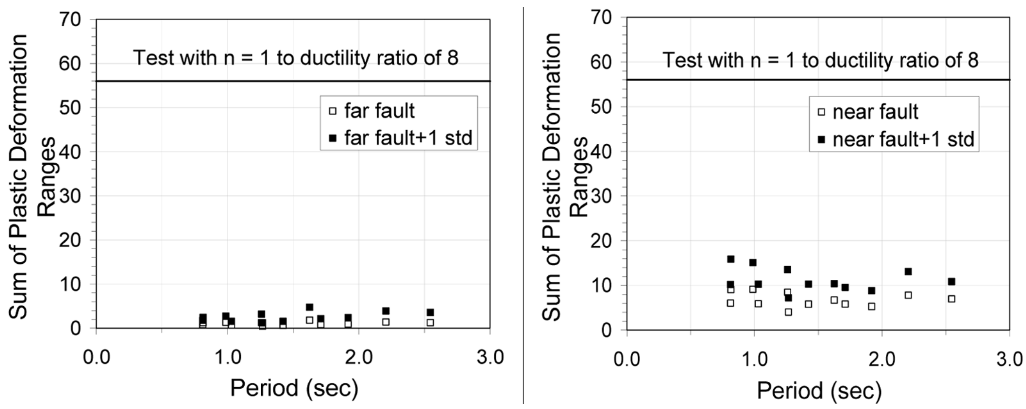

Fig. 7 Vibration Period versus NP relationship for $6.3 < \mu < 10.4$

the cracked section flexural stiffness, versus NP relations are provided for different ductility levels (Figs. 5, 6 and 7). Each point on these graphs corresponds to one column. Each column's NP value is determined by taking the average of NPs obtained for forty earthquakes in the group. NP calculated for the cyclic load that consists of one cycle for each ductility level has also been illustrated on these graphs by a horizontal bold line. For all ductility levels, near-fault earthquake types provide a much larger number of inelastic loading cycles than far-fault earthquake types. Except for the lower ductility range ($3.3 < \mu < 4.8$), there is no dependence of NP on the natural vibration period of the columns.

5. Analytical works and results

Krawinkler (1996) asserted that the cyclic demands for structures depend on a great number of variables and that a unique quasi-static load pattern will always be a compromise, but one that should be conservative for most practical cases. He described how a reasonable and generally conservative loading history is attained. In his depiction, the total number of inelastic excursions (N) should be represented as an average, and that the cumulative damage should be represented conservatively. Consideration should also be given to the fact that small inelastic excursions are much more frequent than large ones.

The values given in Table 5 are the inelastic excursion numbers which are classified into eight groups obtained from the NTHA of the columns. In a NTHA, if the peak displacement response exceeds δ_y, one should consider that it is being an inelastic excursion and the corresponding yield ductility is $\mu_i = \delta_i/\delta_y$. In Fig. 8, for a selected column and EQ record, the total inelastic excursion number observed as 6 and its classification for ductility ranges are as follows: Two for $1 < \mu_i < 2$, one for $2 < \mu_i < 3$, one for $3 < \mu_i < 4$ and two for $4 < \mu_i < 5$. The average and average-plus-one standard deviation of the observed inelastic excursions for each yield ductility range obtained from 36 columns × 40 EQ records = 1440 total analyses for each EQ type are given in the table. Half of the values given in Table 5 might be used as the number of full cycles.

Figs. 9 and 10 are the graphical representation of Table 5 for far-fault and near-fault earthquake types, respectively. The horizontal axis corresponds to response ductility and the vertical axis indicates average values of the observed inelastic excursions. To acquire more conservative results, the standard deviation is considered in the unfavorable side. To compare the number of inelastic excursions obtained from NTHAs with quasi-static test results, two horizontal line ($n = 1$ and $n = 3$) are also added to the graphics. They correspond to the traditional displacement patterns in which one and three cycles for each ductility level are repeating. Three cyclic quasi-static displacement

Table 5 Averages of the observed inelastic excursions

Earthquake	Number of Nonlinear Excursions							
	δ_y-$2\delta_y$	$2\delta_y$-$3\delta_y$	$3\delta_y$-$4\delta_y$	$4\delta_y$-$5\delta_y$	$5\delta_y$-$6\delta_y$	$6\delta_y$-$7\delta_y$	$7\delta_y$-$8\delta_y$	$8\delta_y$-$9\delta_y$
Far-fault	1.94	1.46	1.47	1.25	1.00			
Far-fault+1std	3.23	2.00	1.82	1.38	1.00			
Near-fault	2.55	1.62	1.17	1.12	1.19	1.00	1.13	1.00
Near-fault+1std	4.57	2.52	1.51	1.32	1.39	1.00	1.30	1.00

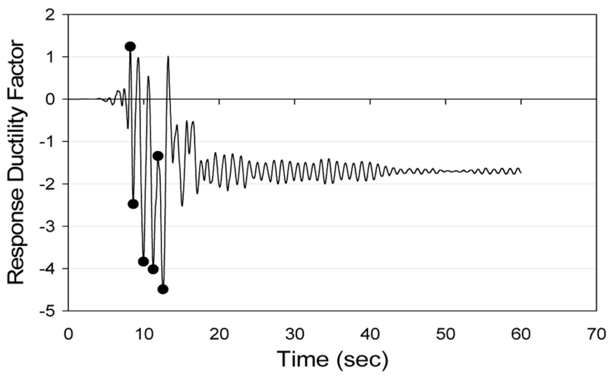

Fig. 8 Definition of inelastic excursions

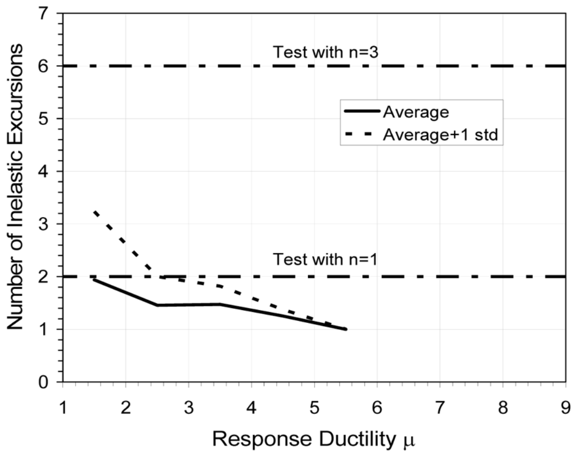

Fig. 9 The number of inelastic excursions for far-fault earthquake types

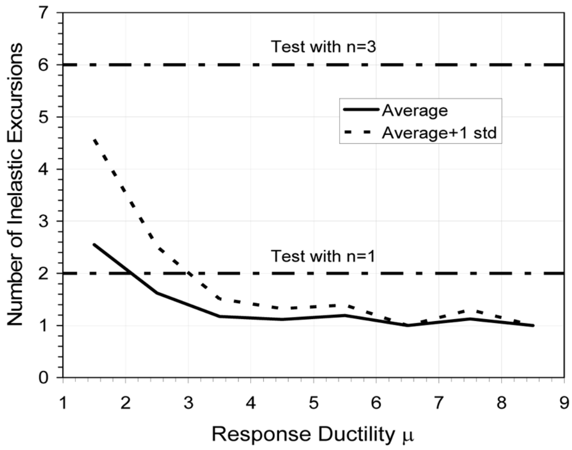

Fig. 10 The number of inelastic excursions for near-fault earthquake types

patterns provide much larger number of inelastic loading cycles than the actual seismic behavior of RC columns.

The proposed number of inelastic cycles is given in Table 6. In the determination of the number of inelastic cycles, it is aimed to stay in the conservative side. Based on the number of inelastic cycles, the proposed loading pattern consisting of a series of stepwise increasing displacement cycles is given in Fig. 11. In the case of far-fault earthquake types, the maximum displacement ductility is defined as $6\delta_y$. The cycles are symmetric in peak displacement. The effect of displacement sequence that has not yet been established through research is out of scope. Prior to the first yielding of the column, the quasi-static test may be controlled by load rather than displacement.

NTHAs are performed for each column, so the peak displacement and cumulative DI values are obtained. The analyses were ended whether DI equals to 1.0 for the displacement target or the maximum displacement response of the earthquake is observed. Afterwards each column was statically loaded by the "proposed" and also with two others namely "one cyclic" and "three cyclic"

Table 6 Number of inelastic cycles

Earthquake Type	Number of Cycles							
	δ_y-$2\delta_y$	$2\delta_y$-$3\delta_y$	$3\delta_y$-$4\delta_y$	$4\delta_y$-$5\delta_y$	$5\delta_y$-$6\delta_y$	$6\delta_y$-$7\delta_y$	$7\delta_y$-$8\delta_y$	$8\delta_y$-$9\delta_y$
Far-fault	1	1	1	1	1			
Far-fault+1std	2	2	1	1	1			
Near-fault	2	1	1	1	1	1	1	1
Near-fault+1std	3	2	1	1	1	1	1	1

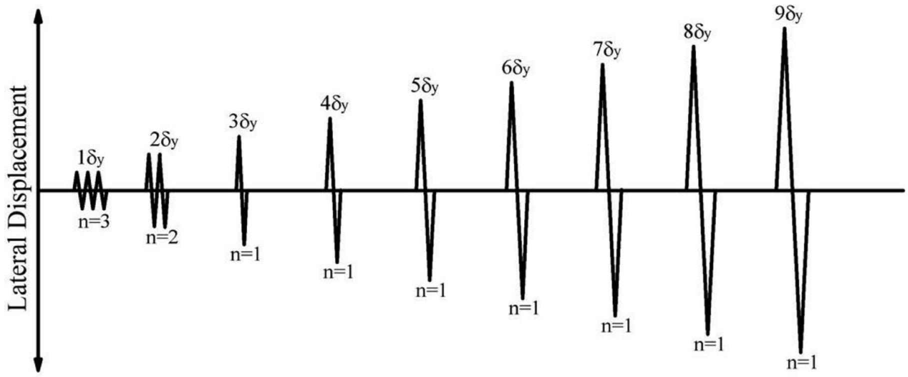

Fig. 11 The recommended quasi-static displacement pattern

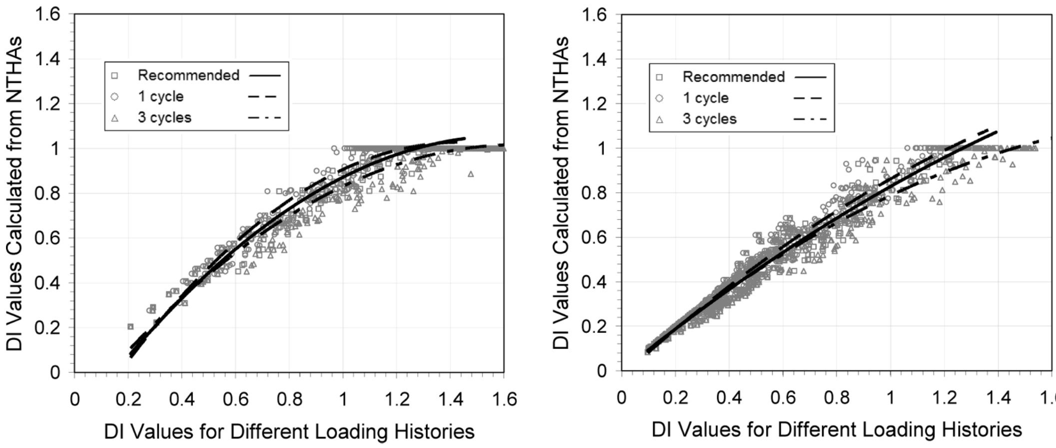

Fig. 12 DI comparisons for $3.3 < \mu < 4.8$ (Left: Near-Fault, Right: Far-Fault)

quasi-static cyclic displacement patterns, until reaching to the peak displacement observed in NTHA performed for an EQ record. The abscissa and ordinate of any point on Figs. 12, 13 and 14 represent DIs obtained from nonlinear static analysis and NTHA, respectively. There exist three DIs obtained for quasi-static cyclic displacement patterns corresponding to a specific NTHA demand. There are $12 \times 40 \times 3 = 1440$ points on each graph; 12, 40 and 3 correspond to the number of

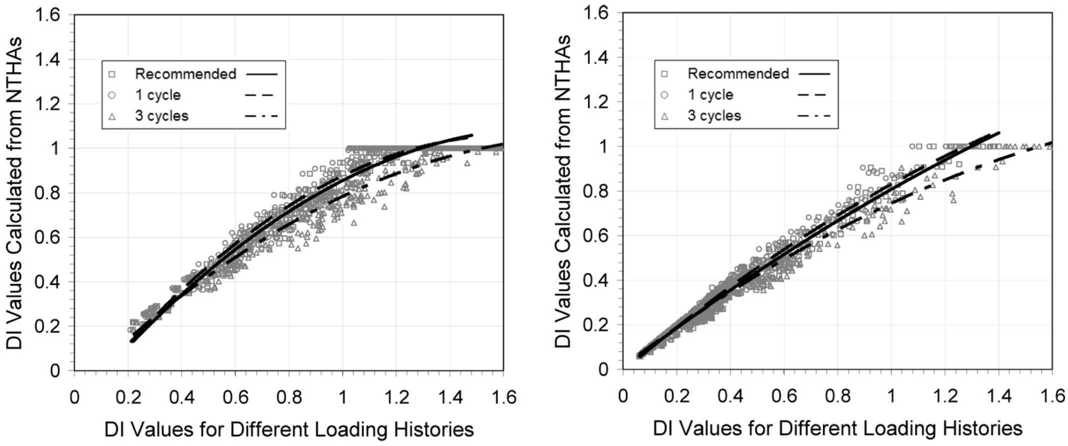

Fig. 13 DI comparisons for 4.9 < μ < 6.2 (Left: Near-Fault, Right: Far-Fault)

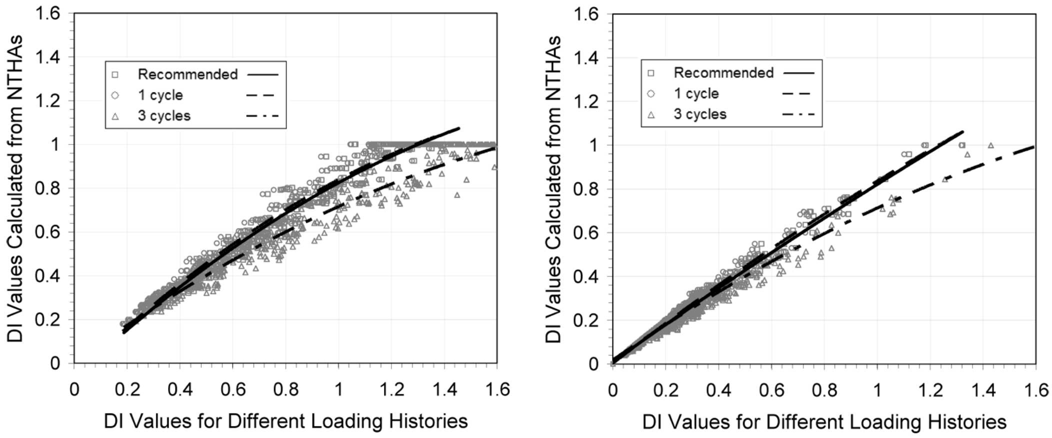

Fig. 14 DI comparisons for 6.3 < μ < 10.4 (Left: Near-Fault, Right: Far-Fault)

columns in the ductility range, number of earthquake records, and number of quasi-static displacement patterns, respectively.

Trend lines for the three quasi-static displacement patterns are also included to the diagrams. An evaluation of the trend lines shows that all the quasi-static displacement patterns generate more damage than the dynamic analyses. When the ductility range of the column is higher, the discrepancy between "three cycles" and the others becomes larger. The trend lines obtained in the far-fault case are almost linear, but those of the near-fault case are curvilinear.

The effect of column cross section on the proposed quasi-static displacement pattern is evaluated in Fig. 15 through a comparison of DI values obtained from non-linear static and dynamic analysis. The longitudinal reinforcement ratio ρ_v is 1% and 3% for the left and right graphs, respectively. The axial force ratio of 10% is valid for both graphs. There is no significant discrepancy between the trend lines representing the results.

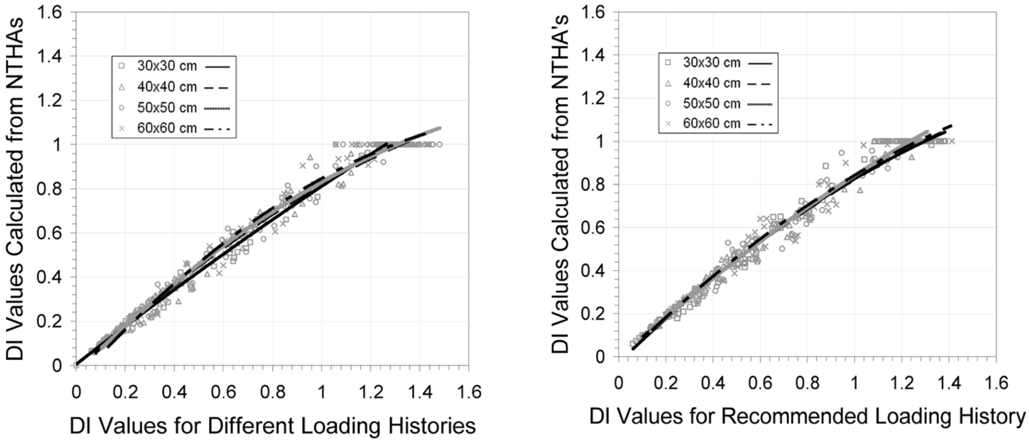

Fig. 15 The effect of column cross section (ρ_v = 1% for the left and 3% for the right)

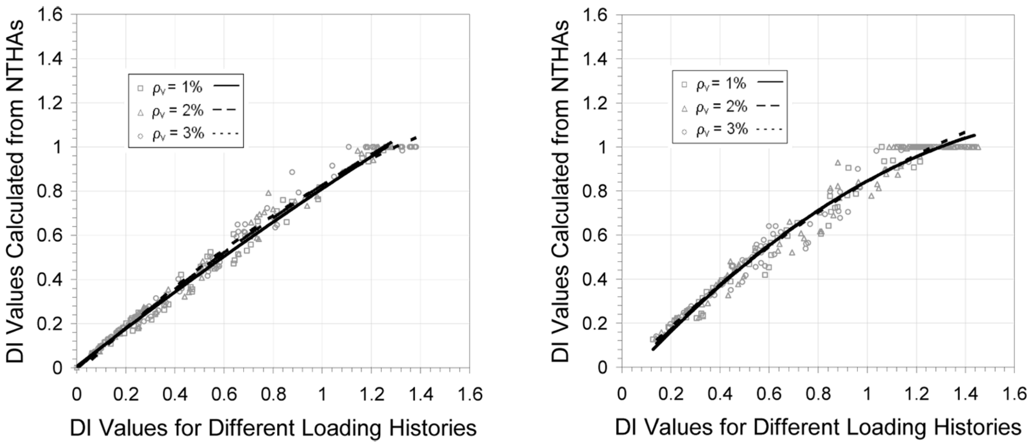

Fig. 16 The effect of ρ_v (30 × 30 cm for the left and 60 × 60 cm for the right)

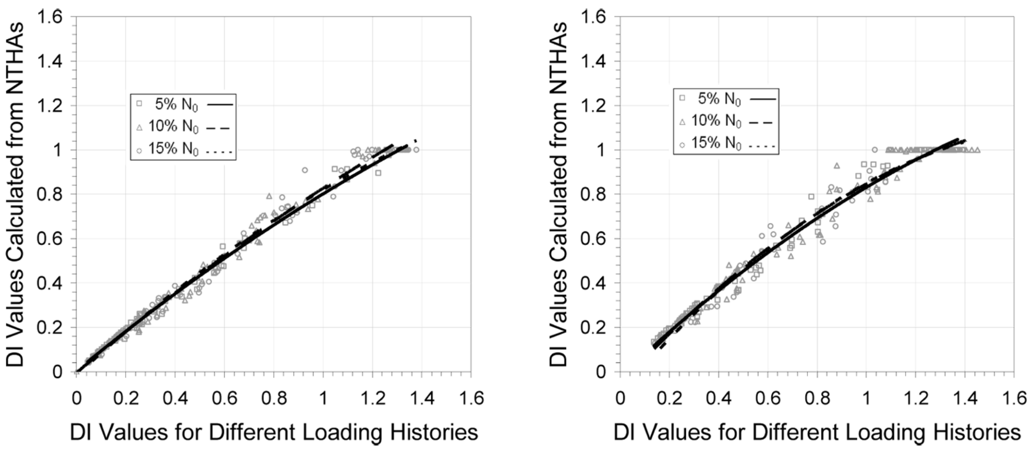

Fig. 17 The effect of axial force ratio (30 × 30 cm for the left and 60 × 60 cm for the right)

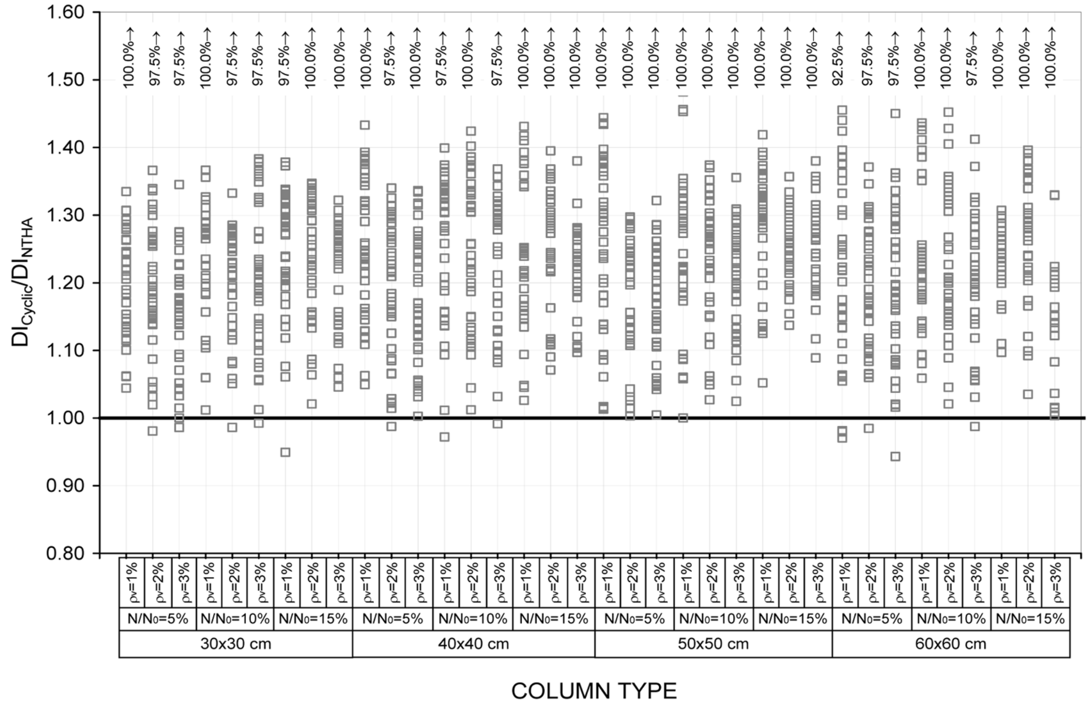

Fig. 18 DI ratios for near-fault earthquakes

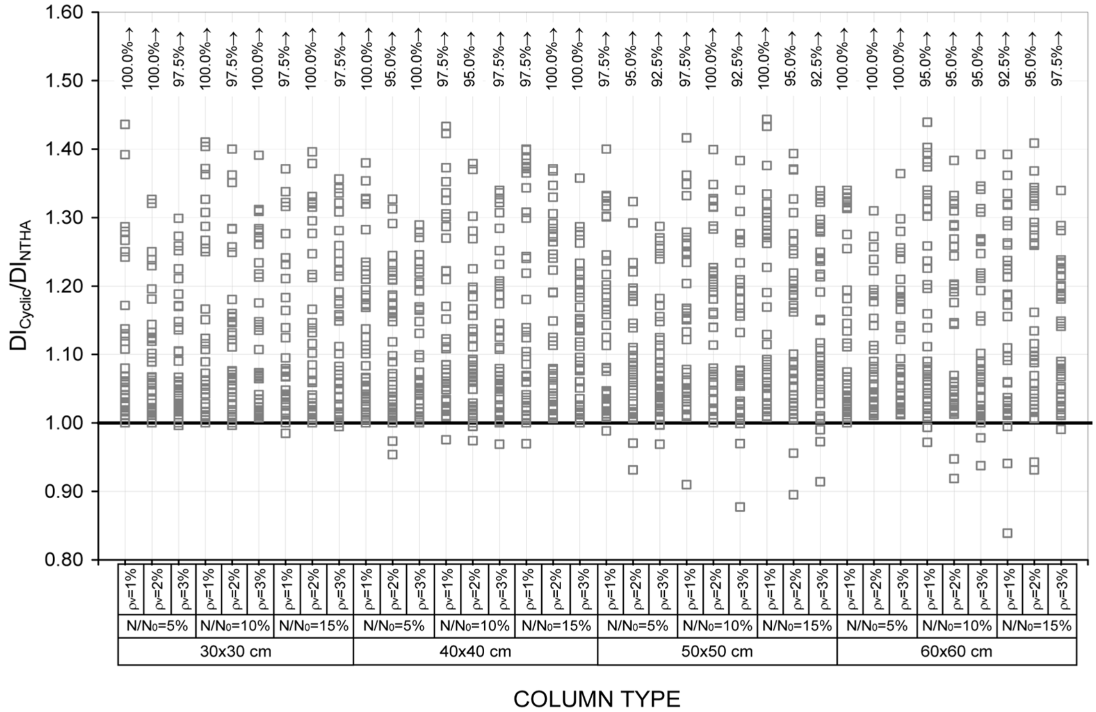

Fig. 19 DI ratios for far-fault earthquakes

The effect of longitudinal reinforcement ratio ρ_v on the proposed quasi-static displacement pattern is assessed in Fig. 16. The column cross sections are 30 × 30 cm and 60 × 60 cm for the left and right graphs, respectively. The axial force ratio is 10% for both cases. The trend lines representing the results are riding each other.

The effect of axial force ratio on the proposed quasi-static displacement pattern is evaluated in Fig. 17. The column cross sections are 30 × 30 cm and 60 × 60 cm for the left and right graphs, respectively. The longitudinal reinforcement ratio ρ_v is fixed at 2%. In a similar manner, the discrepancy between the trend lines representing the results is trivial.

Ratios of DIs are illustrated in Figs. 18 and 19 for near-fault and far-fault earthquake types, respectively. DI_{cyclic} stands for the cumulative damage to the column through the proposed quasi-static displacement pattern. DI_{NTHA} denotes cumulative damage achieved in NTHAs. There are forty points for each parameter set. As seen from Figs. 18 and 19, with the exception of very few columns the DI_{cyclic}/DI_{NTHA} ratio is greater than 1.0. Therefore, one can state with confidence that the proposed quasi-static displacement pattern estimates the cumulative damage conservatively.

6. Conclusions

A quasi-static cyclic displacement pattern consisting of a series of stepwise increasing deformation cycles as shown in Fig. 11 for well-confined, flexure-dominated RC columns has been suggested. The number of cycles to be applied preceding the proposed displacement pattern should be enough to obtain stable and reliable values of stiffness properties.

The analytical results demonstrated that far-fault earthquake types cause a much smaller number of inelastic excursions than near-fault earthquake types. The maximum excursion ranges for far-fault and near-fault earthquakes are $\pm5\delta_y$ to $\pm6\delta_y$ and $\pm8\delta_y$ to $\pm9\delta_y$, respectively.

The current study demonstrated that the traditional quasi-static loading pattern, in which three cycles for each ductility level are repeating, provides large cumulative damage, especially for relatively ductile columns.

Utilization of the proposed quasi-static cyclic displacement pattern to evaluate the earthquake performance of columns will reduce the total test duration considerably.

The proposed quasi-static cyclic displacement pattern which is based on the cumulative damage concept obtained for well-confined, flexure-dominated RC columns may not be fully applicable for other RC structural components or structural components made from other materials.

Acknowledgements

The authors wish to thank Professor Faruk Karadogan and Research Assistant Serkan Z. Yuce for making available the experimental data used in this study.

References

Ambraseys, N., Smit, P., Sigbjornsson, R., Suhadolc, P. and Margaris, B. (2002), "Internet-site for european strong-motion data", European Commission, Research-Directorate General, Environment and Climate

Programme.

ATC-24 (1992), "Guidelines for cyclic seismic testing of components of steel structures", Applied Technology Council, Redwood City, California.

COSMOS Virtual Data Center, Consortium of Organizations for Strong Motion Observation Systems (COSMOS), University of California. <http://db.cosmos-eq.org/scripts/default.plx/>

FEMA 461 (2007), "Interim protocols for determining seismic performance characteristics of structural and nonstructural components", Federal Emergency Management Agency.

Gatto, K. and Uang, C.M. (2003), "Effects of loading protocol on the cyclic response of woodframe shearwalls", *J. Struct. Eng.-ASCE*, **129**(10), 1384-1393.

Hwang, T. and Scribner, C. (1984), "R/C member cyclic response during various loadings", *J. Struct. Eng.*, **110**(3), 477-489.

Karadogan, F., Yuksel, E., Yuce, S., Taskın, K. and Saruhan, H. (2006), "The experimental studies on original and retrofitted precast columns", Technical Report, Istanbul Technical University. (in Turkish)

Kawashima, K. and Koyama, T. (1988), "Effect of number of loading cycles on dynamic characteristics of reinforced concrete bridge pier columns", *Proceedings of JSCE*, No.392/I-9, 205-213.

Kawashima, K., Buckle, I. and Loh, C.H. (2002), "Loading history for quasi-static cyclic tests for reinforced concrete bridge columns", *Proceedings of the 3rd International Workshop on Performance-Based Seismic Design and Retrofit of Transportation Facilities*, Tokyo Institute of Technology, Tokyo, Japan.

Krawinkler, H. (1996), "Cyclic loading histories for seismic experimentation on structural components", *Earthq. Spectra*, **12**(1), 1-12.

Krawinkler, H., Gupta, A., Medina, R. and Luco, N. (2000), "Development of loading histories for testing of steel beam-to-column assemblies," SAC Background Report SAC/BD-00/10.

Park, Y.J. and Ang, A.H. (1985), "Mechanistic seismic damage model for reinforced concrete", *J. Struct. Eng.-ASCE*, **111**(4), 722-739.

Park, Y.J., Ang, A.H. and Wen, Y.K. (1985), "Seismic damage analysis of reinforced concrete buildings", *J. Struct. Eng.-ASCE*, **111**(4), 740-757.

Park, Y.J., Reinhorn, A.M. and Kunnath, S.K. (1987), IDARC: Inelastic Damage Analysis of Reinforced Concrete Frame - Shear-Wall Structures. Technical Report NCEER-87-0008, State University of New York at Buffalo.

PEER Strong Motion Database (2000), Pacific Earthquake Engineering Research Center, California. <http://peer.berkeley.edu/smcat/>

Reinhorn, A.M., Kunnath, S.K. and Valles, R.E. (2006), "A program for the inelastic damage analysis of buildings", IDARC2D V6.1, State University of New York at Buffalo.

SAC Steel Project (1997), "Impulsive Near-Field Earthquake Ground Motions. Richmond", CA. <http://www.sacsteel.org/>

Seismosignal V.3.2, (2006), Seismo Soft. <http://www.seismosoft.com/>

Shafei, B. and Zareian, F. (2008), "Development of a quasi-static loading protocol for displacement sensitive nonstructural building components", *Proceedings of the 14th World Conference on Earthquake Engineering*, Beijing, China.

Surmeli, M. (2008), "Performance evaluation of precast columns under seismic excitation", M.Sc. Thesis, Graduate School of Istanbul Technical University.

TKYHP, Turkey National Strong Ground Motion Program, General Directorate of Disaster Affairs. <http://angora.deprem.gov.tr/>

Tsuno, K. and Park, R. (2004), "Experimental study of reinforced concrete bridge piers subjected to bi-directional quasi-static loading", *Proc. JSCE*, **21**(1), 11-26.

Turkish Seismic Code (2007), Regulations on Structures Constructed in Disaster Regions. Ankara. Ministry of Public Works and Settlement.

USGS, United States National Strong Motion Project (NSMP), U.S, Geological Survey. Denver. <http://agram.wr.usgs.gov/>

XTRACT V3.0.7 (2006), Cross-sectional Structural Analysis of Components. Imbsen Software Systems. Sacramento, CA.

Yuksel, E. and Surmeli, M. (2010), "Failure analysis of one-story precast structures for near-fault and far-fault strong ground motions", *Bull. Earthq. Eng.*, **8**, 937-953.